Materials Advances

ROYAL SOCIETY OF CHEMISTRY

PAPER

View Article Online
View Journal | View Issue

Cite this: *Mater. Adv.*, 2022, 3, 8260

Hybrid organic–inorganic perovskites as microwave radiation switches†

Olesia I. Kucheriv, [a] Viktor V. Oliynyk,[b] Volodymyr V. Zagorodnii,[b] Vilen L. Launets,[b] Igor O. Fritsky [a] and Il'ya A. Gural'skiy [a]*[a]

Received 3rd June 2022,
Accepted 2nd September 2022

DOI: 10.1039/d2ma00633b

rsc.li/materials-advances

Hybrid organic–inorganic perovskites are an intensively growing class of functional materials that attract much attention due to their various practical and important functionalities. In this paper, we show the ability of two hybrid perovskites, namely $CH_3NH_3PbI_3$ and $(C_5H_{11}NH_3)_2PbI_4$, to act as phase transition (PT) microwave switches. Microwave switching was studied as a consequence of PTs which occur at technologically attractive temperatures – slightly above room temperature: 330 K for $CH_3NH_3PbI_3$ and 320 K for $(C_5H_{11}NH_3)_2PbI_4$. It was found that, at selected frequencies, $(C_5H_{11}NH_3)_2PbI_4$ is characterized by a very high transmission value of −0.4 dB which changes to −4.4 dB upon transition to a high-temperature phase. On the contrary, the transmission of $CH_3NH_3PbI_3$ at room temperature is deficient (−25 dB) and increases just slightly upon transformation into a high-temperature phase. The microwave absorption changes by 38% for $(C_5H_{11}NH_3)_2PbI_4$ and by 0.6% for $CH_3NH_3PbI_3$ at selected frequencies. Notably, absorption in $(C_5H_{11}NH_3)_2PbI_4$ changes from 9.9% at room temperature to 48.2% above the temperature of the PT, which is a five-fold increase. Our measurements show that $CH_3NH_3PbI_3$ is rather suitable for application as microwave absorber, while $(C_5H_{11}NH_3)_2PbI_4$ can be efficiently used as an active material in microwave switches.

Introduction

Metal halide organic–inorganic perovskites represent an actively growing class of multipurpose materials. Classical 3D hybrid halide perovskites are compounds of the general formula ABX_3, where A is an organic cation, B is a divalent cation (typically Pb^{2+}, Sn^{2+}, Ge^{2+}) and X is halogen. They attract attention mainly as semiconductors and have been recently investigated for their ability to serve as active elements in solar cells,[1–5] lasers,[6,7] photodetectors,[8,9] light emitting diodes,[10,11] for water splitting[12,13] *etc.* One of the most studied and applied hybrid perovskites nowadays is $CH_3NH_3PbI_3$ because of the outstanding combination of relatively simple and low-cost fabrication techniques, tunability of band gap through chemical modification,[14] high carrier mobility, long lifetime, long diffusion length, and high absorption coefficient, *etc.*[15]

A relatively easy way to modify the chemical composition of perovskites is through the introduction of different organic cations and inorganic anions, which lead to obtaining hundreds of compounds, belonging to this class.[16] Besides 3D hybrid perovskites, 2D analogues of this class have gained widespread popularity. These perovskites feature 2D halometallic layers separated by bulky organic cations.[17] 2D hybrid perovskites are much more common than the 3D ones due to the large variety of suitable cations that can support 2D structures.[18]

A lot of hybrid organic–inorganic perovskites demonstrate temperature-induced structural PTs, which are mostly associated with rearrangement of organic cations or tilting of BX_6 octahedra.[18] Importantly, many physical properties of hybrid perovskites are associated with PTs, for example, dielectric transitions and ferroelectric transitions.[19] At the same time, phase-transition hybrid perovskites can potentially be used as molecular switches of very different functionalities.

It has been repeatedly shown that hybrid organic–inorganic perovskites can serve as efficient absorbers of microwave radiation.[20–22] However, their ability to switch microwave radiation upon a PT has majorly remained outside the scope of attention of researchers. There are several reports on the change of permittivity of hybrid perovskites in the GHz range[23,24] upon PT which show prospects of microwave switching.

One of the challenges of today's industries that utilize microwave radiation (5G, SatCom applications, *etc.*) is the development of efficient reconfigurable components that can be tuned to support variable frequency bands and communication standards. In highly integrated devices, which have to

[a] *Department of Chemistry, Taras Shevchenko National University of Kyiv, 64 Volodymyrska St., Kyiv 01601, Ukraine. E-mail: illia.guralskyi@univ.kiev.ua*
[b] *Educational and Scientific Institute of High Technologies, Taras Shevchenko National University of Kyiv, 64 Volodymyrska St., Kyiv 01601, Ukraine*

† Electronic supplementary information (ESI) available. See DOI: https://doi.org/10.1039/d2ma00633b

support multiple communication standards simultaneously, a reconfigurable filter can help reduce the total number of filters which would benefit the miniaturization of devices. Switching with smart materials is considered to be an efficient alternative to classical techniques for microwave switching, such as p–i–n diodes,[25,26] microelectromechanical systems,[27,28] field effect transistors,[29,30] *etc.* For example, successful switching has been shown by dielectric anisotropy control in liquid crystals.[31] Additionally, there are numerous examples of microwave switching by PTs in germanium halogenides[32] and vanadium dioxide.[33,34] Our team has recently shown the ability of Fe^{II} coordination compounds with thermally-induced spin crossover to operate as efficient microwave switches.[35,36] In this paper we study capabilities of two hybrid organic–inorganic perovskites to switch microwave radiation: 3D semiconductive perovskite $CH_3NH_3PbI_3$ (**C_1PbI**) and a 2D perovskite $(C_5H_{11}NH_3)_2PbI_4$ (**C_5PbI**).[37]

Results and discussion

Phase transitions

C_1PbI and **C_5PbI** were chosen due to the temperatures of PTs. While both perovskites display multiple PTs, we focused our attention in this work on microwave switching during the transitions that occur at technologically attractive temperatures – slightly above room temperature. PTs in both the obtained samples were studied using differential scanning calorimetry (Fig. 1). **C_1PbI** displayed a temperature-induced PT at 333 K in heating mode and at 327 K in cooling mode. According to the previously reported data, this transition corresponded to the change in crystallographic space group from *I*4/*mcm* to *Pm*$\bar{3}$*m* at low and high temperature, respectively.[38] In the case of **C_5PbI**, PT occurred at 323 K upon heating and 311 K upon cooling. According to Billing *et al.*, this PT corresponded to the structural change, namely space group $P2_1/a$ at low-temperature changes to

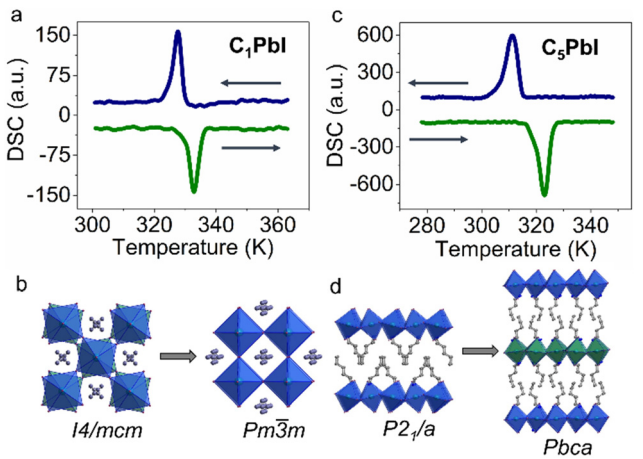

Fig. 1 DSC curves of **C_1PbI** (a) and **C_5PbI** (c) showing temperature-induced PT associated with structural changes. Crystal structures of **C_1PbI** (b) and **C_5PbI** (d) showing different packing before and after PT. Crystal structures are depicted using CIF files provided in ref. 37 and 39 for **C_1PbI** and **C_5PbI**, respectively.

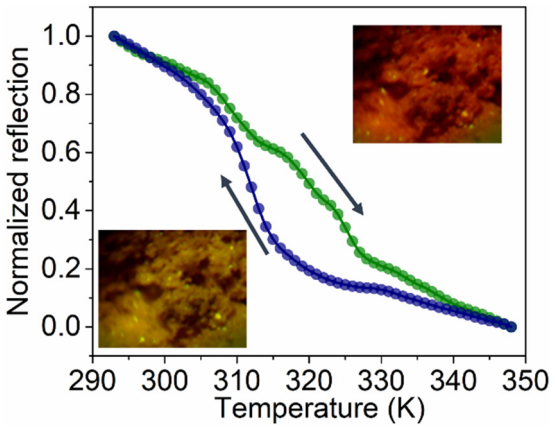

Fig. 2 Optical reflectance measurements for **C_5PbI**, displaying a color change associated with PT.

Pbca at high temperature.[37] PT in **C_5PbI** was additionally monitored by following optical reflection (Fig. 2), which showed similar temperatures of transition. Such an experiment was not possible for **C_1PbI** because of its black color which essentially does not change upon PT.

Microwave transmission and reflection

When a microwave radiation falls on a material, the incident energy is divided into three parts: energy that is reflected back, transmitted through, and absorbed by a material.[40]

To fully characterize the way **C_1PbI** and **C_5PbI** interacted with microwave radiation, both the microwave transmission and reflection were measured using a scalar network analyzer. The S_{11} parameter corresponded to the reflection of microwave radiation at port 1 which occurred due to impedance mismatch. When S_{11} is equal to 0 dB, complete reflection from port 1 occurred, while S_{11} values of −10 dB or lesser corresponded to a low reflection, indicating good impedance matching. S_{21} parameter characterized microwave transmission from port 1 to 2: S_{21} value of 0 dB indicated a 100% transmission without losses, while all the values below 0 dB indicated losses of the signal.[34]

Powdered samples of **C_1PbI** and **C_5PbI** were pressed inside the Ka-band rectangular hollow waveguide. The spectral variations of microwave transmission and reflection have been measured in 26.0–37.5 GHz frequency ranges at variable temperatures. **C_1PbI** at room temperature (291 K) was characterized by very low transmission values, which ranged in between (−24.5) and (−29.5) dB depending on frequency (Fig. 3a). Such low values meant that microwave radiation was essentially not transmitted through the sample. Microwave transmission through **C_1PbI** increased slightly upon heating to the temperatures of PT; it was found to lie in the range of (−17.2)–(−25.7) dB at 348 K. Temperature variation in the microwave transmission for **C_1PbI** at 30.0 GHz is shown in Fig. 3b.

Microwave transmission measurements for **C_5PbI** revealed a completely different result. Very high values of transmission (Fig. 3c) were observed at room temperature. Importantly,

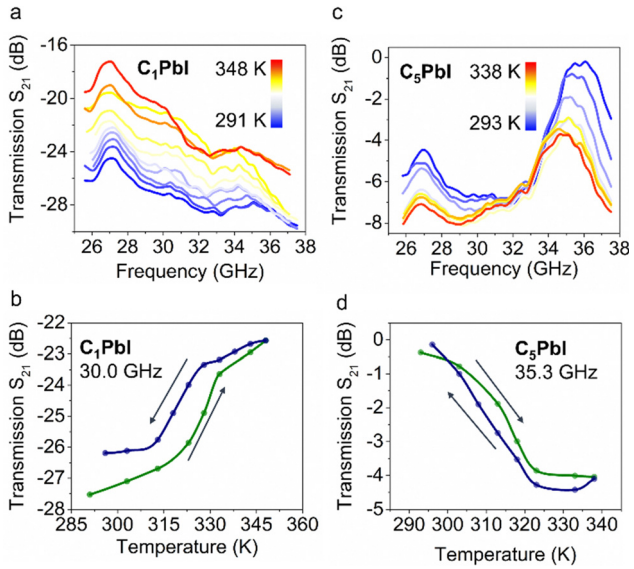

Fig. 3 Spectral variation in microwave transmission (dB) for **C_1PbI** (a) and **C_5PbI** (c) with temperature obtained in a matched waveguide. Extracted values of transmission *vs.* temperature for **C_1PbI** (b) and **C_5PbI** (d) are given for selected frequencies. These curves demonstrate a microwave transmission change upon PT.

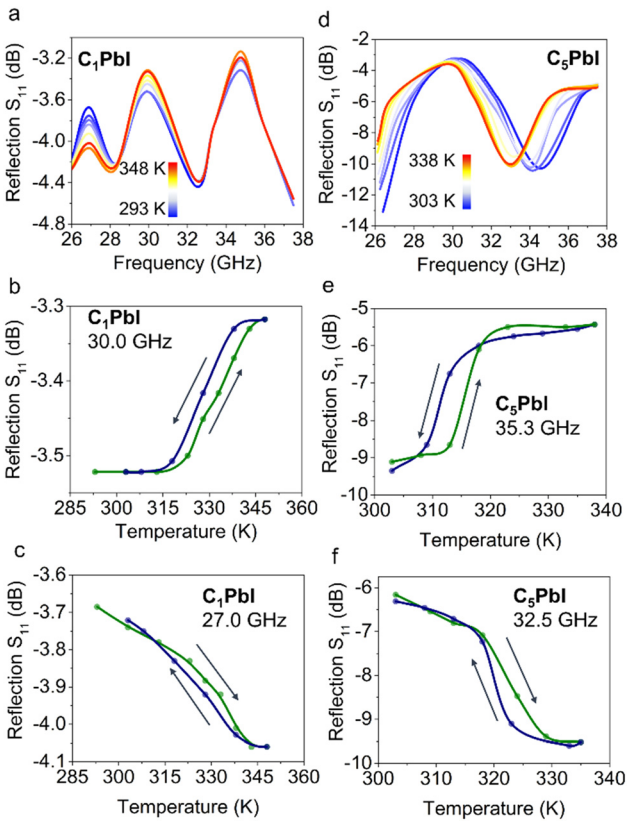

Fig. 4 Spectral variation of microwave reflection (dB) of **C_1PbI** (a) and **C_5PbI** (d) with temperature. Reflection *vs.* temperature plots for **C_1PbI** (b and c) and **C_5PbI** (e and f) at selected frequencies are plotted.

microwave transmission was −0.4 dB at 35.3 GHz and 293 K, which indicated almost complete transmission of radiation through the sample with minimal losses. An abrupt decrease in the transmission was observed upon heating to 338 K (Fig. 3d). S_{21} equaled −4.4 dB in the high-temperature phase, which indicated considerable rise of absorption and/or reflection by the sample. Some slight differences in transition temperatures and hysteresis width observed in microwave transmission and DSC experiments were associated with the settling mode of S_{21} measurements. Large-sized samples and the waveguide itself required thermalization for 10–15 min at each temperature before the measurements. Some small temperature oscillations altered the hysteresis in the measured curve. Small kinetic effects could also be suggested.

A small temperature-dependent drift of microwave transmission was noted in the regions above and below PT. In order to investigate temperature effects on S_{21} that were not associated with PT, this parameter was studied for $(C_4H_9NH_3)_2PbBr_4$ (**C_4PbBr**) above room temperature. The material crystalized in *Pbca* space group at room temperature and was isostructural to the high-temperature form of **C_5PbI**.[41,42] DSC measurements revealed the absence of any PT in the studied temperature range for **C_4PbBr** (Fig. S1, ESI†). Temperature dependent measurements of microwave transmission (Fig. S2, ESI†) showed a slight gradual decrease from −3.6 dB at 301 K to −4.6 dB at 348 K (defined at 35.3 GHz). Such a drift of S_{21} with temperature was possibly associated with slight changes of permittivity with temperature in this sample.[43] Simultaneously, **C_5PbI** S_{21} switching was intensified by structural deformations due to the PT and the observed decrease in transmission significantly exceeded pure temperature-related effects.

As for the microwave reflection, S_{11} spectra of **C_1PbI** were characterized by the presence of reflection bands with minima at 28.3 and 32.5 GHz (Fig. 4a). Transition to the high-temperature phase was followed by a slight change in the peaks' intensity while their position remained almost unchanged. Depending on the frequency, either a decrease or an increase in reflection could be achieved (Fig. 4b and c).

For example, S_{11} was −3.52 dB at 30 GHz and room temperature (293 K). This value increased slightly upon heating with transition to the high-temperature (348 K) phase; it reached −3.32 dB. If analysis was performed at 27 GHz, reflection at room temperature equaled −3.7 dB. This value decreased to −4.0 dB under heating.

Similar to microwave transmission, reflection measurements revealed more significant changes for **C_5PbI** upon PT. This perovskite was characterized by the presence of a S_{11} band at 34.6 GHz. During the transition to high-temperature phase, a significant shift of band's position towards lower frequencies (up to 33.0 GHz) was observed. Such shift can indicate the increase of permittivity of this material upon PT. Either a decrease or increase in reflection can be observed for **C_5PbI** depending on the operating frequency. For example, S_{11} equals −9.1 dB at 35.4 GHz and 303 K, indicating low reflection from the sample. This correlates well with very high transmission at the same frequency and temperature. With the transition to the

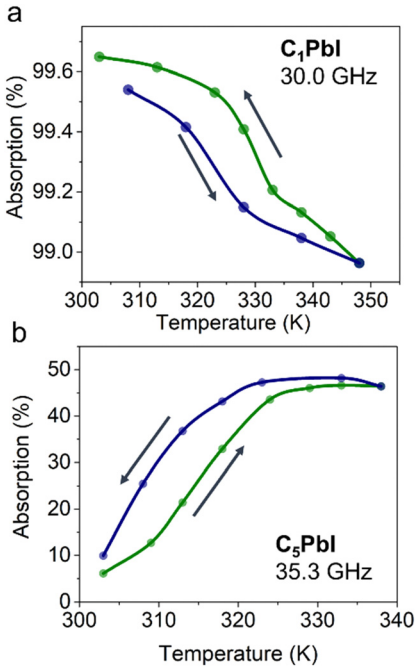

Fig. 5 Absorption of microwave radiation by **C_1PbI** (a) and **C_5PbI** (b) at selected fixed frequencies. The dependencies show that **C_5PbI** can effectively switch microwave radiation, while **C_1PbI** should be rather used as a microwave absorber.

high-temperature phase (338 K), S_{11} increases to −5.4 dB at this frequency. An inverse effect was observed at 32.5 GHz: S_{11} decreased from −6.2 to −9.5 dB upon transition from the low-temperature (303 K) to the high-temperature phase (338 K).

Effective microwave absorption value of materials can be described by the following equation:[44,45]

$$A_{\text{eff}} = \frac{1 - T - R}{1 - R}, \quad (1)$$

where T is transmission and R is reflection.

Changes in effective absorption upon PT for **C_1PbI** and **C_5PbI** at selected frequencies are shown in Fig. 5. The absorption for **C_1PbI** sample was approx. 99.6% at 303 K (at 30.0 GHz). During the temperature-induced PT, this value decreased slightly and reached 99.0%. These observations show that **C_1PbI** is rather suitable for application as a microwave absorber, while its switching ability associated with a PT above room temperature is poor.

At the same time, effective absorption of **C_5PbI** sample was 9.9% at 303 K. This parameter drastically increases with a transition to the high-temperature phase and reaches 48.2% at 338 K. Importantly, the microwave radiation absorption in **C_5PbI** increases by a factor of five, which means that **C_5PbI** can be prospective material for microwave switches.

Such a strong difference in absorption between the two investigated HOIPs can be associated with the difference in their crystal structures. The 3D packing of **C_1PbI** is known to be responsible for its semiconducting properties, which, in turn, induce strong microwave absorption of this material. Simultaneously, **C_5PbI** with its 2D crystal structure does not display any

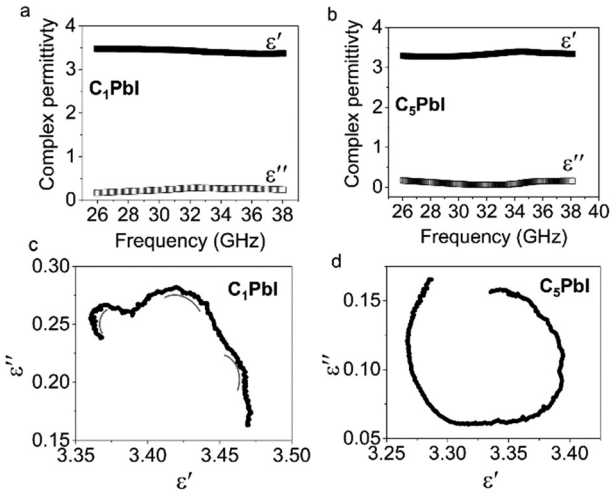

Fig. 6 Dependence of complex permittivity (ε' and ε'') of **C_1PbI** (a) and **C_5PbI** (b) on frequency. Cole–Cole plots for **C_1PbI** (c) and **C_5PbI** (d) in 26–38 GHz frequency range.

semiconducting properties, and, thus, its microwave absorption is considerably lower. At the same time, during structural transition to the high-temperature phase of **C_5PbI**, an increase in cell volume and, consequently, a decrease in the material's density occurs. This effect, in turn, may facilitate orientation of dipoles, leading to an increase in microwave absorption due to dielectric relaxation mechanisms.

In order to study the mechanism of microwave absorption in **C_1PbI** and **C_5PbI**, complex dielectric permittivity of these materials was measured as a function of frequency at room temperature (Fig. 6a and b). It can be seen that the ε' values of both the materials displayed minor changes depending on frequency. The real part of **C_1PbI** permittivity was 3.47 at 26 GHz; it slightly dropped with an increase in frequency and reached 3.37 at 38 GHz. The imaginary part of **C_1PbI** permittivity was 0.16 at 26 GHz, which changed to 0.28 and 0.24 at 32.4 and 38.0 GHz, respectively. The values found in this experiment were close to previously shown ones for **C_1PbI** in 2–18 GHz range at room temperature.[46]

The real part of permittivity for **C_5PbI** was close to the value obtained for **C_1PbI**: ε' of this perovskite was 3.29 at 26 GHz, 3.39 at 34.0, and 3.33 at 38.0 GHz. At the same time, ε'' values of **C_5PbI** were lower than measured values for **C_1PbI**. The imaginary part of permittivity for pentylammonium perovskite was 0.16 at 26 GHz, ε'' first dropped with a frequency increase and reached its minimum value of 0.06 at 33 GHz. With further increase in frequency, ε'' slightly increased again and reached 0.16 at 38 GHz. These dependences of the complex permittivity on frequency cannot be described *via* any simple model, *i.e.*, more information on the mechanism of dielectric relaxation is necessary.

Absorption of microwave radiation in such materials is typically realized due to dielectric losses caused by dipole orientation polarization. In case of the studied materials, free organic cations in the pores of inorganic frameworks could serve as efficient polarization centers. Those dipoles re-orient

under the influence of thermal motion upon removal of external electromagnetic field; such process can be described as dipolar polarization relaxation.[40] In such systems, dependence between ε' and ε'' can be described by the Debye theory:

$$\left(\varepsilon' - \frac{\varepsilon_s + \varepsilon_\infty}{2}\right)^2 + (\varepsilon'')^2 = \left(\frac{\varepsilon_s - \varepsilon_\infty}{2}\right)^2,$$

where ε_∞ is the relative permittivity at infinite frequency and ε_s is the static permittivity. Cole–Cole semicircles, which can be observed in ε' *vs.* ε'' dependence shown in Fig. 6c and d, represent the Debye relaxation process. Importantly, each semicircle describes one relaxation process. **C_1PbI** demonstrated three semicircles in the investigated frequency range, while in the case of **C_5PbI**, only one typical Cole–Cole semicircle could be observed. Therefore, a higher number of relaxation processes and higher values of ε'' with similar values of ε' explain the higher absorptivity of **C_1PbI**.

Transmission and reflection spectra obtained in VNA measurements at room temperature for **C_1PbI** and **C_5PbI** are shown in Fig. S4 (ESI†). While the values observed for **C_5PbI** were similar for scalar and vector measurements, S_{21} parameters observed for **C_1PbI** in the second experiment were lower. The observed distinctions were associated with different types of waveguides used in two measurements (rectangular waveguide for scalar temperature-dependent experiments and coaxial waveguide for vector measurements) in which significantly different dispersion and attenuation were realized. Additionally, dilution with PMMA polymer, which was used for fabrication of toroidal samples for VNA, could also influence transmission/reflection values.

To the best of our knowledge, the current work was the first study of temperature-dependent microwave transmission/reflection of hybrid perovskites, which exhibited PT. There have been several previous studies on temperature-dependent permittivity of 2D[24] perovskites at 9.5 GHz and 3D[24] perovskites at 90 GHz, where PT were observed. In both cases, an increase in microwave permittivity was observed upon heating, with a transition occurring from a more ordered to a less ordered state. Also, there were multiple reports on significant absorption of microwave frequency radiation by hybrid perovskites at room temperature.[21,22,46,47] Thus, changes in permittivity in the microwave range upon PT and high absorption ability, in combination with a huge variety of accessible hybrid organic–inorganic perovskites, made this class of materials very attractive for use in different microwave technologies. Considering the low number of studies published on hybrid perovskites interaction with microwave radiation and the promising results obtained in the current work, further investigations in this direction are worth performing.

Experimental

Materials

Lead iodide was purchased from Acros organics, pentylamine, buthylamine and methylammonium iodide were purchased from UkrOrgSyntez Ltd and used as received.

Synthesis

Methylammonium lead iodide $CH_3NH_3PbI_3$ (**C_1PbI**) was obtained according to a slightly modified procedure offered by Weber *et al.* in 1978.[48] Two grams of PbI_2 (4.3 mmol, 1 eq.) was dissolved in 6 ml of concentrated HI with heating. Thereafter, 828 mg (5.16 mmol, 1.2 eq.) of CH_3NH_3I was added to 1 ml of HI. The mixture was transferred to an oven and kept at 45 °C for 10 h. During this time, a black precipitate was formed. After that, the mixture was centrifuged and dried in air. Yield was 30% (800 mg).

Pentylammonium lead iodide $(C_5H_{11}NH_3)_2PbI_4$ (**C_5PbI**) was obtained according to a slightly modified procedure offered by Billing *et al.* in 2007.[37] A gram of PbI_2 (2.2 mmol, 1 eq.) was dissolved in 3 ml of concentrated HI with heating. Thereafter, 452 mg (5.28 mmol, 2.4 eq.) of $C_5H_{11}NH_2$ in 1 ml of HI was added. Bright-orange precipitate was formed immediately. The mixture was cooled down, centrifuged and dried in air. The yield was 95% (1.86 g).

Butylammonium lead bromide $(C_4H_9NH_3)_2PbBr_4$ (**C_4PbBr**) was obtained according to a slightly modified procedure offered by Karunadasa *et al.* in 2017.[42] $PbBr_2$ (750 mg, 2.0 mmol, 1 eq.) was dissolved in 2 ml of concentrated HBr with heating. Thereafter, 350 mg (4.8 mmol, 2.4 eq.) of $C_4H_9NH_2$ was added to 1 ml of HBr. White crystals were formed after cooling the solution, collected, dried on air and ground for further experiments. Yield was 70% (740 mg).

Measurements

Optical reflectance measurements were conducted using a Linkam DSC 600 temperature-controlled microscope stage cryostat and Optica SZM-1 stereomicroscope equipped with a Sigeta UCMOS 1300 camera. The processing of images was performed with ImageJ software. Reflectance measurements were performed at a heating/cooling rate of 10 K min^{-1}.

Differential scanning calorimetry measurements were performed with a Linkam DSC 600. DSC profiles were recorded with a heating/cooling rate of 10 K min^{-1}.

Microwave transmission/reflection measurements were carried out with a P2-65 scalar microwave network analyzer operating in the Ka frequency band. An analyzer was equipped with a hollow rectangular waveguide (7.20 mm × 3.40 mm). The powdered samples of **C_1PbI** and **C_5PbI** were pressed into rectangular pellets inside the waveguide by applying *ca.* 20 MPa pressure (d = 6.00 mm). The waveguide filled with a perovskite sample was heated with an external thermostat for temperature-dependent measurements. The experiments were conducted in a settling mode at which the waveguide with the sample inside was thermalized for 10–15 min at each temperature value before collecting the measurements. Narrow thermal intervals for microwave measurements were selected for each perovskite from the preceding optical and DSC experiments.

Complex dielectric permittivity was measured using Keysight PNA N5227A vector network analyser. For this experiment, **C_1PbI** and **C_5PbI** were mixed with 50% of inert poly(methyl methacrylate) matrix and cut as coaxial rings of toroidal shape

with an outer diameter of 1.85 mm and inner diameter of 0.82 mm. Thickness of both samples was 6 mm. Permittivity measurements of PMMA matrix are given in Fig. S3 (ESI†).

The PXRD patterns were acquired on Shimadzu XRD-6000 diffractometer using Cu-Kα radiation (10–50 °C range, 0.05 °C steps) (Fig. S5 and S6, ESI†). The measurements revealed some differences in peak intensities in comparison to simulated PXRD patterns. Such observations can be explained by preferential orientation in the samples. However, the same way of sample preparation used for both PXRD and microwave transmission/reflection experiments suggested the possibility that orientation of samples in the two experiments was similar.

Conclusions

Here we show the ability of hybrid organic–inorganic perovskites to change their microwave absorption during the temperature-induced structural PT. Methylammonium lead iodide displayed very high absorption around room temperature, which decreased by less than 1% upon PT, showing that this perovskite was rather suitable for use as an absorber, but not a switch. Pentylammoniun lead iodide displayed moderate absorption at room temperature, which increased five-fold upon PT, which highlighted this material as an efficient microwave switch. These results make an important contribution to the creation of preliminary dataset of microwave absorbing and switching properties of hybrid organic–inorganic perovskites.

Author contributions

Olesia I. Kucheriv, Volodymyr V. Zagorodnii, Vilen L. Launets – investigation, Viktor V. Oliynyk and Igor O. Fritsky – data curation, Il'ya A. Gural'skiy – conceptualization and supervision. All authors contributed to the writing of this manuscript.

Conflicts of interest

There are no conflicts to declare.

Acknowledgements

This work was supported by the Ministry of Education and Science of Ukraine with grant no. 22BF037-09 and a grant from the Ministry of Education and Science of Ukraine for perspective development of a scientific direction ''Mathematical Sciences and Natural Sciences'' at Taras Shevchenko National University of Kyiv, no. 21BNN-06. Authors also acknowledge the courage of Armed Forces of Ukraine which made the submission of this manuscript possible.

Notes and references

1 A. Kojima, K. Teshima, Y. Shirai and T. Miyasaka, *J. Am. Chem. Soc.*, 2009, **131**, 6050–6051.
2 N. J. Jeon, J. H. Noh, W. S. Yang, Y. C. Kim, S. Ryu, J. Seo and S. Il Seok, *Nature*, 2015, **517**, 476–480.
3 H.-S. Kim, C.-R. Lee, J.-H. Im, K.-B. Lee, T. Moehl, A. Marchioro, S.-J. Moon, R. Humphry-Baker, J.-H. Yum, J. E. Moser, M. Grätzel and N.-G. Park, *Sci. Rep.*, 2012, **2**, 591.
4 L. Etgar, P. Gao, Z. Xue, Q. Peng, A. K. Chandiran, B. Liu, M. K. Nazeeruddin and M. Grätzel, *J. Am. Chem. Soc.*, 2012, **134**, 17396–17399.
5 W. S. Yang, J. H. Noh, N. J. Jeon, Y. C. Kim, S. Ryu, J. Seo and S. Il Seok, *Science*, 2015, **348**, 1234–1237.
6 H. Zhu, Y. Fu, F. Meng, X. Wu, Z. Gong, Q. Ding, M. V. Gustafsson, M. T. Trinh, S. Jin and X.-Y. Zhu, *Nat. Mater.*, 2015, **14**, 636–642.
7 G. Xing, N. Mathews, S. S. Lim, N. Yantara, X. Liu, D. Sabba, M. Grätzel, S. Mhaisalkar and T. C. Sum, *Nat. Mater.*, 2014, **13**, 476–480.
8 F. Khorramshahi, A. G. Woughter, M. K. Ram, I. Kymissis and A. Takshi, *Adv. Electron. Mater.*, 2019, **5**, 1900518.
9 Z. Duan, J. Ning, M. Chen, Y. Xiong, W. Yang, F. Xiao, S. V. Kershaw, N. Zhao, S. Xiao and A. L. Rogach, *ACS Appl. Mater. Interfaces*, 2020, **12**, 35201–35210.
10 Y. Cao, N. Wang, H. Tian, J. Guo, Y. Wei, H. Chen, Y. Miao, W. Zou, K. Pan, Y. He, H. Cao, Y. Ke, M. Xu, Y. Wang, M. Yang, K. Du, Z. Fu, D. Kong, D. Dai, Y. Jin, G. Li, H. Li, Q. Peng, J. Wang and W. Huang, *Nature*, 2018, **562**, 249–253.
11 M. Lu, Y. Zhang, S. Wang, J. Guo, W. W. Yu and A. L. Rogach, *Adv. Funct. Mater.*, 2019, **29**, 1902008.
12 J. Luo, J.-H. Im, M. T. Mayer, M. Schreier, M. K. Nazeeruddin, N.-G. Park, S. D. Tilley, H. J. Fan and M. Grätzel, *Science*, 2014, **345**, 1593–1596.
13 S. Singh, H. Chen, S. Shahrokhi, L. P. Wang, C.-H. Lin, L. Hu, X. Guan, A. Tricoli, Z. J. Xu and T. Wu, *ACS Energy Lett.*, 2020, **5**, 1487–1497.
14 T. Jesper Jacobsson, J.-P. Correa-Baena, M. Pazoki, M. Saliba, K. Schenk, M. Grätzel and A. Hagfeldt, *Energy Environ. Sci.*, 2016, **9**, 1706–1724.
15 J. Y. Kim, J. W. Lee, H. S. Jung, H. Shin and N. G. Park, *Chem. Rev.*, 2020, **120**, 7867–7918.
16 E. I. Marchenko, S. A. Fateev, A. A. Petrov, V. V. Korolev, A. Mitrofanov, A. V. Petrov, E. A. Goodilin and A. B. Tarasov, *Chem. Mater.*, 2020, **32**, 7383–7388.
17 J. Wong and K. Yang, *Sol. RRL*, 2021, **5**, 2000395.
18 W. Li, A. Stroppa, Z. Wang and S. Gao, *Hybrid Organic–Inorganic Perovskites*, Wiley, 2020.
19 C. Shi, X. Bin Han and W. Zhang, *Coord. Chem. Rev.*, 2019, **378**, 561–576.
20 V. M. Caselli, M. Fischer, D. Meggiolaro, E. Mosconi, F. De Angelis, S. D. Stranks, A. Baumann, V. Dyakonov, E. M. Hutter and T. J. Savenije, *J. Phys. Chem. Lett.*, 2019, **10**, 5128–5134.
21 H. Guo, J. Yang, B. Pu, H. Chen, Y. Li, Z. Wang and X. Niu, *J. Mater. Chem. C*, 2018, **6**, 4201–4207.
22 C. Zhang, C. Mu, J. Xiang, B. Wang, F. Wen, J. Song, C. Wang and Z. Liu, *J. Mater. Sci.*, 2017, **52**, 13023–13032.
23 H. Zangar, J. L. Miane, C. Courseille, N. B. Chanh, M. Couzi and Y. Mlik, *Phys. Status Solidi*, 1989, **115**, 107–118.
24 A. Poglitsch and D. Weber, *J. Chem. Phys.*, 1987, **87**, 6373–6378.

25 X. Zhang, X. Zou, C. W. Tang and K. M. Lau, *Phys. Status Solidi*, 2017, **214**, 1600817.
26 G. Upadhyay and V. S. Tripathi, *Microwave. Opt. Technol. Lett.*, 2017, **59**, 1454–1460.
27 C. Dehoff, A. Hennings, C. Kügeler, T. Schneller and U. Böttger, *Phys. Status Solidi*, 2011, **208**, 343–356.
28 L.-Y. Ma, N. Soin, M. H. Mohd Daut and S. F. Wan Muhamad Hatta, *IEEE Access*, 2019, **7**, 107506–107522.
29 D. P. Nguyen, A. Pham and F. Aryanfar, *IEEE Microwave Wireless. Componen. Lett.*, 2016, **26**, 696–698.
30 A. Quddious, M. A. B. Abbasi, M. A. Antoniades, P. Vryonides, V. Fusco and S. Nikolaou, *IEEE Trans. Antennas Propag.*, 2020, **68**, 5872–5881.
31 D. C. Zografopoulos, A. Ferraro and R. Beccherelli, *Adv. Mater. Technol.*, 2018, **4**, 1800447.
32 P. Mahanta, M. Munna and R. Coutu, *Technologies*, 2018, **6**, 48.
33 J. Wang, B. Xiong, R. Peng, C. Li, B. Hou, C. Chen, Y. Liu and M. Wang, *Small*, 2021, **17**, 2101282.
34 S. Yang, M. Vaseem and A. Shamim, *Adv. Mater. Technol.*, 2019, **4**, 1800276.
35 O. I. Kucheriv, V. V. Oliynyk, V. V. Zagorodnii, V. L. Launets and I. A. Gural'skiy, *Sci. Rep.*, 2016, **6**, 38334.
36 O. I. Kucheriv, V. V. Oliynyk, V. V. Zagorodnii, V. L. Launets, O. V. Penkivska, I. O. Fritsky and I. A. Gural'skiy, *RSC Adv.*, 2020, **10**, 21621–21628.
37 D. G. Billing and A. Lemmerer, *Acta Crystallogr., Sect. B: Struct. Sci.*, 2007, **63**, 735–747.
38 P. S. Whitfield, N. Herron, W. E. Guise, K. Page, Y. Q. Cheng, I. Milas and M. K. Crawford, *Sci. Rep.*, 2016, **6**, 35685.
39 Y. Ren, I. W. H. Ostwald, X. Wang, G. T. McCandless and J. Y. Chan, *Cryst. Growth Des.*, 2016, **16**, 2945–2951.
40 B. Wang, Q. Wu, Y. Fu and T. Liu, *J. Mater. Sci. Technol.*, 2021, **86**, 91–109.
41 L. Dou, A. B. Wong, Y. Yu, M. Lai, N. Kornienko, S. W. Eaton, A. Fu, C. G. Bischak, J. Ma, T. Ding, N. S. Ginsberg, L.-W. Wang, A. P. Alivisatos and P. Yang, *Science*, 2015, **349**, 1518–1521.
42 M. D. Smith, A. Jaffe, E. R. Dohner, A. M. Lindenberg and H. I. Karunadasa, *Chem. Sci.*, 2017, **8**, 4497–4504.
43 E. E. Havinga, *J. Phys. Chem. Solids*, 1961, **18**, 253–255.
44 H.-B. Zhang, Q. Yan, W.-G. Zheng, Z. He and Z.-Z. Yu, *ACS Appl. Mater. Interfaces*, 2011, **3**, 918–924.
45 B. Zhao, M. Hamidinejad, S. Wang, P. Bai, R. Che, R. Zhang and C. B. Park, *J. Mater. Chem. A*, 2021, **9**, 8896–8949.
46 Z. Zhang, Z. Xiong, Y. Yao, D. Wang, Z. Yang, P. Zhang, Q. Zhao and W. Zhou, *Adv. Funct. Mater.*, 2022, 2206053.
47 H. Lin, M. Green, L. J. Xu, X. Chen and B. Ma, *Adv. Mater. Interfaces*, 2020, **7**, 3–9.
48 D. Weber, *Z. Naturforsch., B: Anorg. Chem., Org. Chem.*, 1978, **33**, 1443–1445.